xxxx-xx-xxxx

1D Numerical and experimental investigations of an Ultra-Lean Pre-Chamber Engine

Author, co-author (Do NOT enter this information. It will be pulled from participant tab in MyTechZone)

Affiliation (Do NOT enter this information. It will be pulled from participant tab in MyTechZone)

Abstract

In recent years, lean burn gasoline Spark-Ignition (SI) engines have been a major subject of investigations. With this solution, in fact, it is possible to simultaneously reduce NO_x raw emissions and fuel consumption due to decreased heat losses, higher thermodynamic efficiency and enhanced knock resistance. However, the real applicability of this technique is strongly limited by the increase in cyclic variation and the occurrence of misfire, which are typical for the combustion of homogeneous lean air/fuel mixtures. The employment of a Pre-Chamber (PC), in which the combustion begins before proceeding in the main combustion chamber, has already shown the capability of significantly extending the lean burn limit.

In this work, the potential of an ultra-lean PC SI engine for a decisive improvement of the thermal efficiency is presented by means of numerical and experimental analyses. The SI engine is experimentally investigated with and without the employment of the PC with the aim to analyze the real gain of this innovative combustion system. For both configurations, the engine is tested at various speeds, loads and air-fuel ratios. A commercial gasoline fuel is directly injected into the main-chamber, while the PC is fed in a passive or active mode. Compressed natural gas or hydrogen is used in the actual case.

A 1D model of the engine under study is implemented in a commercial modeling framework and is integrated with "in-house developed" sub-models for the simulation of the combustion and turbulence phenomena occurring in this unconventional engine. The numerical approach proves to reproduce the experimental data with good accuracy, without requiring any case-dependent tuning of the model constants.

Both the numerical and experimental results show an improvement of the indicated thermal efficiency of the active pre-chamber, compared to the conventional ignition device, especially at high loads and low speeds. The injection of hydrogen into the pre-chamber leads to significant benefit only with very lean mixtures. With the passive fueling of the PC, the lean burning limit is less extended, with the consequent lower improvement potential for the thermal efficiency.

Introduction

Nowadays, atmospheric air pollution is a considerable problem, especially with reference to the Internal Combustion Engines (ICEs), also examining the global warming and particularly the greenhouse gas due to the vehicles. To face this challenge and also because of the more stringent legislations [1], car manufacturers are improving their knowledge on alternative technical solutions to face this challenge, without penalizing the high-standards of engine performance. One of the most severe targets concern the CO_2 emission reduction of the vehicle fleet [2], both for the Worldwide harmonized Light vehicle Test Cycle (WLTC) and real driving operations.

On one hand, there is a long-term solution, under development, that concerns the advent of pure electric or fuel cell vehicles, but their growth has slowed by the limited availability of electricity or hydrogen produced from renewable energy sources [3,4]. On the other hand, a short-term solution foresees, as a transitional path, an evolution from pure thermal engines to hybrid powertrains. Although the future powertrain architecture will be electrified, a further effort to improve the efficiency of the ICEs is mandatory. Indeed, a highly efficient engine allows to limit the size of the electrical component, such as battery and electric machines. Additionally, when the vehicle power demand is high and if the electric units are unable to totally supply this last, an engine with limited pollutant and CO_2 emissions is necessary.

Regarding Spark-Ignition (SI) engines, high efficiency downsized architectures with VVT/VVA devices [5] are now state-of-the-art. Additional benefits can be obtained using advanced anti-knock measures, such as variable compression ratio [6], cooled exhaust gas recirculation [7], and water injection [8]. The fuel consumption advantages are nevertheless rather limited if those architectures are tested along the homologation driving cycle required by the WLTP [9].

Consequently, in the recent years the car manufactures are moving towards innovative SI engine concepts, for which the combustion process or the architectures are unconventional. In particular, combustion systems that work with very lean air/fuel mixtures aroused great interest due to the possibility of simultaneously reducing the NO_X raw emissions and the fuel consumption. Operating with very lean mixtures, indeed, allows to reduce NO_x raw emissions, because of lower combustion temperatures [10,11]. Reduced fuel consumption mainly derives from higher ratio of the specific heats, minor heat losses and higher knock resistance. An extremely lean air/fuel mixture also guarantees the limitation of CO and HC emissions, thanks to the excess of air.

It is worth to underline that conventional SI-ICEs are able to work only with a constrained amount of excess of air, so reducing the real advantage of this technique [12]. With the aim to extend lean burning limits, different solutions have been designed in the recent years. Moriyoshi et al. [13] have shown that the twin-tumble of intake flows aiming to generate a slight vertical fuel stratification could reduce the cycle-to-cycle fluctuations, typical of lean combustions. As an alternative, a Spark-Controlled Compression Ignition (SPCCI) is

proposed in [14], altering the modalities in which the ignition and the main combustion phase occur in a conventional SI engine. Firstly, a lean mixture for compression ignition is injected into the combustion chamber. Subsequently, a further fuel injection and the swirl motion are managed to establish a richer air/fuel mixture near the spark plug, aiming to ensure a stable combustion development. Another technique is the utilization as ignition system of a Pre-Chamber (PC). This is characterized by a small volume and is connected to the Main-Chamber (MC) through small orifices. In this system, the combustion process starts at the spark plug located in the pre-chamber. Due to the heat released by the combustion, the PC pressure exceeds the MC one and multiple turbulent jets of hot gas are expelled from the pre-chamber. These jets penetrate the main-chamber, increasing the turbulence and igniting the lean mixture along each jet. The burn rate enhances, improving the combustion stability, even for extremely lean mixtures [15].

The aim of this work is to numerically and experimentally investigate the potential of an ultra-lean pre-chamber SI engine in improving indicated thermal efficiency. In particular, the PC is tested in passive and active modes. The first solution has the benefit of a low cost and engineering straightforwardness. Instead, the latter is particularly interesting due to the possibility to further extend the lean limit, while preserving reasonable cyclic variations [16]. Despite several experimental activities carried out in the recent years on the active pre-chamber [17], the choice of the most suitable fuel to be injected in the PC is still under study. On one hand, gaseous fuels, such as methane [18] and hydrogen [19], or vaporized gasoline [20] guarantee a proper mixture homogenization before the spark event. On the other hand, because of the fuel supply infrastructure for passenger cars, nowadays the liquid gasoline injection remains the most suitable option, although this can cause some risks of a not-perfect mixture formation.

Nowadays, the numerical analysis is an essential part of the development of innovative engine architectures. The most suitable approach to well-describe the interaction between combustion, chemical kinetics, and turbulence in a pre-chamber engine, seems to be 3D CFD codes [21,22,23]. These models show the possibility to explore the effects of the pre-chamber design in terms of volume, nozzle shape, hole size, hole orientation and thickness [24]. Although these analyses exhibit significant results, because of their computational effort, the 3D simulations are usually limited to a reduced number of operating points. Otherwise, 1D models, if coupled with proper phenomenological sub-models of in-cylinder phenomena, can be employed. These represent a proper compromise between reliability and computational effort, allowing to investigate a large number of operating conditions.

In the light of the above consideration, in this work a quasi-dimensional model for an active/passive pre-chamber engine is employed to evaluate the combustion process in this novel architecture. The model aims to give a phenomenological description of all the basic phenomena occurring in an engine fitted with a PC, such as mixture preparation, turbulence evolution, flame area enhancement, burn rate development, etc.

According to the authors' knowledge, only a few predictive phenomenological models, trying to describe the basic physics behind a divided-chamber combustion system, are available in the current literature. A shared thesis is that the control on initial phase of the MC combustion is driven by a conical hot jet released from the PC. For instance, the jet dependency was introduced in [25] by the second Karlovitz number, estimated at the PC hole outlet. Until the Karlovitz number is higher than one, the combustion is controlled by the hot jet turbulent flow generated by the PC. Then, the flame propagation is considered self-sustained because of the in-MC turbulence enhancement, likewise to a conventional engine. In [26], the combustion development was described by an additional entrainment effect. This allows the burning jet to entrain fresh charge, releasing additional heat. The increment of the flame front area has been hypothesized in [27], due to jet penetration. A transition from a drop-shaped flame to a hemisphere is assumed, as a function of a characteristic jet length. These last three approaches, even if including a detailed description of the phenomena occurring in a PC engine, are characterized by a limited validation range due to few operating conditions, especially in terms of air/fuel quality. Unlike in most of the cited works, an original multi-spherical propagation of the flame area in the MC is here proposed. In addition, the presented model is validated against a large range of operating conditions, with different engine loads, speed and as well as relative air/fuel ratios (λ).

This research work is supported by a European H2020 project (EAGLE: https://h2020-eagle.eu/). The project main objective is the experimental and numerical investigation of an ultra-lean combustion concept, applied to a novel engine architecture fitted in a hybrid powertrain. The most ambitious goal is the attainment of very reduced fuel consumption and NO_x and CO_2 emissions, compared to a conventional SI engine.

Firstly, the experimental setup of the examined Single Cylinder Engine (SCE) will be briefly described. The SCE is equipped with either an active pre-chamber, a passive one or a standard spark plug. The active PC is fueled with Compressed Natural Gas (CNG) or hydrogen (H_2), while liquid gasoline is directly injected into the main-chamber. When the PC works in the passive mode, the engine is fueled only with the MC direct injector. Secondly, the quasi-dimensional model will be presented in detail, with emphasis on the combustion description. Finally, the model will be comprehensively validated against the experimental results in terms of pressure traces, burning rates and overall performance. 39 operating points are investigated with the aim to evaluate the model sensitivity to PC configuration, fuel type, engine speed and relative air/fuel ratio (λ) variations.

Experimental setup and tests

The experimental campaign is performed with a Direct Injection (DI) research SCE at the Institute for Combustion Engines (VKA) of the RWTH Aachen University. The existing base engine exhibits high peak pressure capability, external boosting up to 4 bar and variable compression ratios achievable by different piston designs. To carry out the investigations of the EAGLE project, a new top-end was designed. The foremost engine specifications are listed in Table 1.

Combining the long stroke of 90.5 mm and the arrangement of the valves with the intake port and the combustion chamber shape, a charge motion level is achieved, which is comparable to state-of-the-art series production turbocharged engines. It features a tumble flap, which completely shuts off the part of the intake port below the tumble sheet for all investigations presented in this publication.

Figure 1 shows the SCE engine design. The engine is operated with a DI system at 350 bar. It is equipped with a CFD-optimized 4-hole pre-chamber, Figure 1d. The layout process and further results for this pre-chamber have been presented [16].

The design of the cylinder head integrates an ignition module. Based on the size of a generally used M12 spark plugs in passenger car gasoline engines, the outer diameter of the shaft is defined to 12 mm, so that negative influence on the combustion chamber geometry can be avoided. If required, a reduction of the hole to 11 mm is possible. Like shown in the sectional view of Figure 1a-b, the ignition module –

in this case the pre-chamber - is arranged in a central combustion chamber position. As usual with spark plug shafts, cooling water flows around it.

Table 1.Engine main features.

Pre-chamber engine	
Bore, mm	75
Stroke, mm	90.5
Stroke / Bore Ratio	1.206
Displacement, cm^3	399
Peak pressure capability, bar	170
Geometrical compression ratio	13
Injection system	Lateral solenoid, 350 bar
Fuel in main-chamber	DI injector, gasoline RON 98
Fuel in pre-chamber	DI injector CNG: solenoid / H_2: piezo
Pre-chamber volume mm^3	~ 1000
$V_{pre\text{-}chamber}$ / V_{TDC}	~ 3 %
Pre-chamber holes	4 - two pairs of different hole size
$A_{jet\ holes}$ / $V_{pre\text{-}chamber}$, cm^{-1}	~ 0.03
Intake valve opening	3 CAD BTDC (@1mm lift)
Exhaust valve closure	3 CAD ATDC (@1mm lift)
Start of Injection MC	295 CAD BTDC
Start of Injection PC	180-215 CAD BTDC

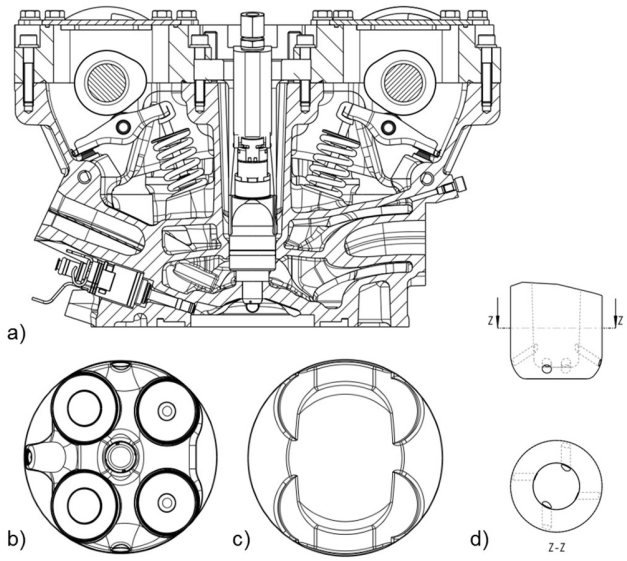

Figure 1. Research engine layout: a) sectional view of cylinder head b) combustion chamber dome c) piston crown for CR=13, d) pre-chamber.

For conventional spark plug operation, the cylinder head is equipped with an adapter instead of the pre-chamber. The adapter realizes the conventional engine design approach with undivided combustion chamber. Thus, this solution is a representative integration in the conventional architecture with spark plug. At the same time, this modular design allows easy replacement of the spark plug by different pre-chambers and a good and direct flow around the pre-chamber with coolant. A single electrode M10 spark plug with heat value of 8 has been used for both pre-chamber (divided combustion chamber) and for conventional spark ignition (undivided combustion chamber) operation.

For active pre-chamber operation, CNG or hydrogen from pressure bottles is used. In case of CNG enrichment, a pressure between 4.5 and 8 bars is set. The injection is done with a solenoid actuated outwards opening injector. For hydrogen injection the pressure is set to 20 bars and a piezo actuated outwards opening injector is applied. For passive operation, the injection into the pre-chamber is switched off. Hence, the same pre-chamber is used in either active or passive mode.

The intake air is conditioned to 30 °C in the intake runner. The pressure upstream of the throttle flap and in the exhaust manifold is controlled to 1.01 bar during throttled operation. While for boosted operation, the pressure in the exhaust system is fixed equal to the one in the intake manifold. The relative air-fuel ratio of the exhaust gas is obtained by the formula of Spindt [28]. The share of the employed fuels (CNG, H_2 and gasoline) is taken into account to establish the correct air/fuel ratios.

Table 2. List of investigated operating points.

Case	**Operating condition rpm @ IMEP**	**Engine**	**λ**	**SA** CAD AFTDC	**MFB_{50}** CAD AFTDC
1	2000 rpm @ 15 bar	STAND	1.0	2.1	23.3
2		STAND	1.2	0.8	25.5
3		STAND	1.4	-4.5	22.1
4		STAND	1.6	-8.8	21.2
5	2000 rpm @ 15 bar	PASSIVE	1.0	11.7	29.1
6		PASSIVE	1.4	2.7	24.1
7	4000 rpm @ 15 bar	PASSIVE	1.0	3.6	20.1
8		PASSIVE	1.4	-3.4	17.6
9	2000 rpm @ 3 bar	CNG	1.6	-15.8	8.6
10	2000 rpm @ 4 bar	CNG	1.0	-11.3	8.1
11		CNG	1.4	-10.8	7.5
12		CNG	1.8	-17.6	7.9
13	2000 rpm @ 10 bar	CNG	1.0	2.3	17.1
14		CNG	1.5	-7.6	7.7
15		CNG	2.0	-16.4	7.1
16	2000 rpm @ 15 bar	CNG	1.0	14.9	33.2
17		CNG	1.4	6.8	25.6
18		CNG	1.8	-3.4	16.7
19		CNG	2.0	-7.5	14.2
20		CNG	2.4	-17.2	9.8
21	2500 rpm@ 12 bar	CNG	1.0	4.0	21.7
22		CNG	1.4	-2.6	15.8
23		CNG	1.8	-13.2	7.78
24		CNG	2.0	-16.4	7.7
25		CNG	2.2	-23.0	7.9
26	2500 rpm @ 6 bar	CNG	2.0	-21.3	7.50
27	3000 rpm @ 13 bar	CNG	1.0	5.8	23.6
28		CNG	1.4	0.3	20.3
29		CNG	1.8	-12.2	9.1
30		CNG	2.0	-16.9	7.8
31		CNG	2.2	-21.0	7.8
32	3000 rpm @ 7 bar	CNG	2.0	-22.7	7.4
33	4000 rpm @ 16 bar	CNG	1.0	11.4	33.7
34		CNG	1.4	5.7	32.2
35		CNG	1.6	2.3	35.2
36	2000 rpm @ 15 bar	H_2	1.4	11.9	29.7
37		H_2	1.8	1.9	20.2
38		H_2	2.0	-4.1	13.8
39		H_2	2.4	-15.7	7.9

At each tested point, the Spark Advance (SA), under knock free operation, is set for optimal combustion phasing (MFB_{50} timing at 7-8 CAD AFTDC), otherwise a delayed ignition timing is set. Pressure measurements are carried out as stated below:

- for the cylinder, two Kistler A6045 B pressure transducers are flush-mounted in the combustion chamber side roof;
- for the pre-chamber, one Kistler 6054 BR pressure transducer is flush mounted in the pre-chamber volume;

- sampling is performed via Kistler charge amplifiers and a FEV combustion analysis system at a resolution of 0.1 CAD;
- for the dynamic intake and exhaust gas pressures, Kistler 4045 A5 pressure transducers are chosen and data are sampled with a resolution of 1 CAD.

Overall, for each operating point, 500 consecutive cycles have been gathered. In order to achieve a comparison with the model, an ensemble average of these cycles is examined. The considered operating points have exhibited satisfactory stability with low IMEP CoV. The latter has been assessed in each operating condition, resulting in rather low values (1-2%), with higher levels at leaner λ. To measure the static pressures and temperatures, conventional pressure transducers and thermocouples, during an averaging interval of 30 s, are adopted. Oil and water conditioning systems enable steady-state operations.

With the aim of developing and validating the model, 39 different operating points, listed in Table 2, are investigated. Different λ sweeps at constant load have been chosen for various engine speeds. This engine operation selection addresses to verify the model predictive potential at changing mixture composition (from stoichiometric to very lean) and turbulence level.

Starting from the acquired pressure traces, the burn rates in the MC are evaluated by a classical two-zone inverse analysis. For the PC engine, the inverse procedure also handles the mass exchange between the chambers. As an example, the burn rates related to points #22 and #24 are shown in Figure 2, referring to a lean and an extremely lean case, respectively. In both points, an initial knee of the burning rate can be observed, related to the combustion speed enhancement due to turbulent jets. Later a slower evolution follows. For the leanest case (#22), strong apparent burning rate fluctuations arise from the beginning of the combustion process, as illustrated in Figure 2. To analyze this phenomenon, the first resonance frequency ($\rho_{m,n}$=1.84) of the main chamber is evaluated according to the Draper's expression [29]:

$$f_0 = \frac{\rho_{m,n}\sqrt{\gamma_{cyl} R T_{cyl}}}{\pi B} \qquad (1)$$

Depending on the gas properties (γ_{cyl} and R) and fluid temperature (T_{cyl}), a value around 6.0 kHz is calculated. A FFT analysis of the MC pressure signal is then performed, showing, in case #22, a peak of the pressure amplitude of about 10 mbar close to f_0 (Figure 3). A similar behavior appears in all the other operating conditions, as well. Peak amplitudes below 1.5 mbar are considered as random noise in the pressure measurements, while values above this threshold can be recognized as physical pressure oscillations. Relevant pressure oscillations only arise when the maximum PC/MC pressure ratio is higher than 1.7-1.8. This is probably due to the occurrence of a chocked flow through the pre-chamber holes. The frequency of such oscillations is close to f_0 in most cases, as shown in Figure 4.

These high-frequency pressure oscillations reflect on the burn rate fluctuations. Since the latter cannot be reproduced by the adopted 0D model, the experimental burn rates are filtered for the simulation assessment (see dotted black lines in Figure 2). As an additional consideration, the frequency range of those pressure oscillations partially overlaps the frequency band typical of knocking combustions (4-20 kHz). For this reason, a refined signal-processing is required, to avoid the misreading of the most common pressure-based knock indicators.

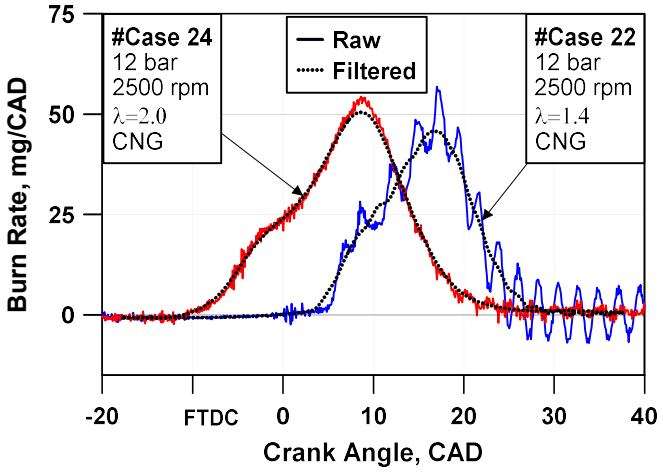

Figure 2. Raw and filtered burn rate in MC at 2500rpm 12 bar IMEP, CNG injected with λ=1.4(blue), λ=2.0 (red).

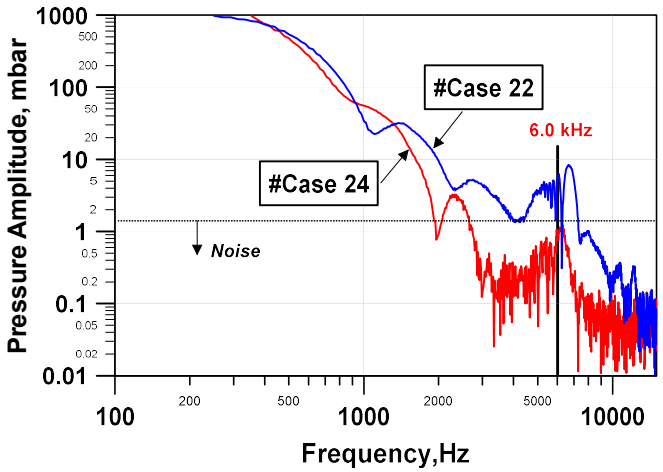

Figure 3. Spectrum of the MC pressure signal at 2500rpm 12 bar IMEP, CNG injected with λ=1.4(blue), λ=2.0 (red).

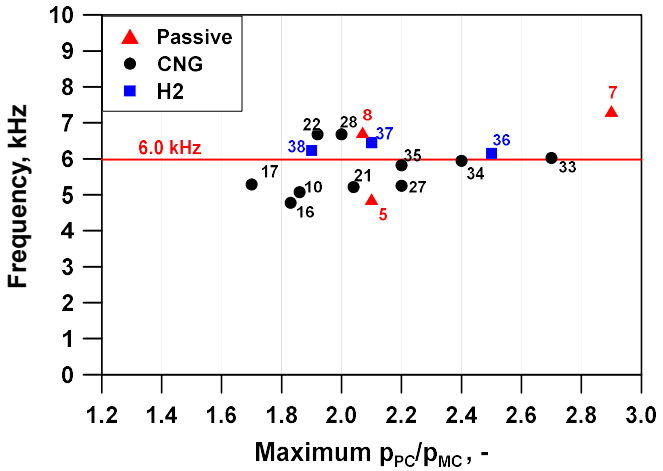

Figure 4 Frequency of the pressure oscillations in the MC vs. the ratio between maximum PC and MC pressures.

Engine model description

Consistently with the experimental layout, a detailed 1D schematization of the tested engine is developed in a commercial modeling framework. The description of the flow inside the intake and the exhaust pipes is based on a 1D approach, whereas phenomenological 0D sub-models are used to reproduce in-cylinder phenomena such as turbulence, combustion and heat transfer.

In particular, the main chamber of the engine is schematized as a variable Zero-Dimensional (0D) volume, connected to the pre-chamber, constant volume, through an orifice. Its diameter is assigned to realize the same overall cross-sectional area as the real PC holes. Mass and energy balance equations are solved in both volumes and a filling/emptying method is used to estimate the mass exchange between them, based on pressure difference, overall cross-sectional area and discharge coefficient of the orifice.

The combustion modelling is based on a two-zone (burned and unburned) schematization, sensing both the chamber geometry and the operating parameters. It is a fractal model, developed by the authors in the last years [30], which has been re-arranged to handle the combustion occurring in both MC and PC.

As well-known, in a conventional SI engine the combustion enhancement is mainly promoted by the turbulence field established during the intake and compression strokes. In a divided-chamber engine, as reported in [16], the combustion in the MC is promoted and supported by the turbulent jets coming from the PC, especially during the early combustion stage. To take into account this phenomenology, the burn rate expression is computed as the sum of two terms, Eq. (2).

$$\left(\frac{dm_b}{dt}\right)_{overall} = \left(\frac{dm_b}{dt}\right)_{fractal} + \left(\frac{dm_b}{dt}\right)_{jet} \quad (2)$$

The first contribution describes the burning rate occurring in a conventional engine, where a corrugated thin flame front, with a surface A_T, propagates locally at laminar speed, S_L:

$$\left(\frac{dm_b}{dt}\right)_{fractal} = \rho_u A_L S_T = \rho_u A_T S_L = \rho_u A_L S_L \frac{A_T}{A_L} \quad (3)$$

ρ_u being the unburned gas density, A_L the laminar area flame area. The wrinkling factor A_T/A_L describes the intensity of the surface corrugations due to the flame/turbulence interaction. According to the fractal theory applied to the flame front geometry [30], the wrinkling factor can be computed based on length scales of the maximum and minimum flame wrinkling, L_{max} and L_{min}, and on the fractal dimension D_3, Eq. (4). This last is estimated by an empirical correlation, depending on the turbulence intensity and laminar flame speed, as reported in [31].

$$\frac{A_T}{A_L} = \left(\frac{L_{max}}{L_{min}}\right)^{D_3-2} \quad (4)$$

The burning rate contribution due to the turbulent jest (second term in Eq. (2)) is computed under the hypothesis that the jets entrains fresh charge (air and fuel) and that the entrained mass progressively burns and releases heat. The heat rate is assumed to be proportional to the difference between the total entrained mass (m_{entr}) and its burned portion ($m_{b,entr}$), and inversely proportional to a characteristic time scale τ, Eq. (5). This last is calculated as the ratio between the Taylor length scale, Λ_T, and the laminar flame speed, S_L. The time derivative of the fresh charge mass entrainment is estimated by a semiempirical correlation [25]. This last, reported in Eq. (6), depends on the mass flow rate out-coming from the PC, $\dot{m}_{jet}$, on a tuning constant c_{jet} and on the density ratio between PC and MC.

$$\left(\frac{dm_b}{dt}\right)_{jet} = \frac{dm_{b,entr}}{dt} = \frac{m_{entr} - m_{b,entr}}{\tau}; \quad \tau = \frac{\Lambda_T}{S_L} \quad (5)$$

$$\frac{dm_{entr}}{dt} = c_{jet}\dot{m}_{jet}\sqrt{\frac{\rho_{PC}}{\rho_{MC}}} \quad (6)$$

The above described model actually applies for a fully developed and freely expanding turbulent flame. During both early flame development and combustion completion, proper modifications are required, as deeply discussed in a previous authors' work [32].

The combustion start in the PC is univocally defined by the spark timing given as a simulation input. On the contrary, the combustion onset in the MC is predicted according to the current flame radius in the PC. As soon as it exceeds a critical value, named r_{crit}, the MC combustion is activated. This parameter, directly correlated to the PC height, can be considered as an additional tuning constant, adjusting the combustion start in the MC.

The laminar flame area A_L in Eq. (3) is calculated at each simulation time step as a function of the burned gas volume and, in the MC case, also of the piston position. For the pre-chamber, it is assumed a smooth spherically shaped propagation with a center moving at a speed proportional to the jet velocity. For the main-chamber, indeed, it is assumed that the flame mainly develops when the turbulent jets have almost dissipated their initial kinetic energy [33]. Fictitious ignition sites are located along each turbulent jet, from which the flame propagates spherically. The position of sphere centers, differently from the PC, is assumed fixed during the combustion development, assigned as an additional input parameter. During the model development, it has verified that a moving center in the MC does not significantly improve the simulation accuracy, but on the other hand increases considerably the computational time. For a conventional engine, the classical assumption of a smooth spherically shaped surface is adopted [30]. To clarify the assumptions about the flame front description, representative flame fronts are depicted in Figure 5 for both conventional and PC ignition devices.

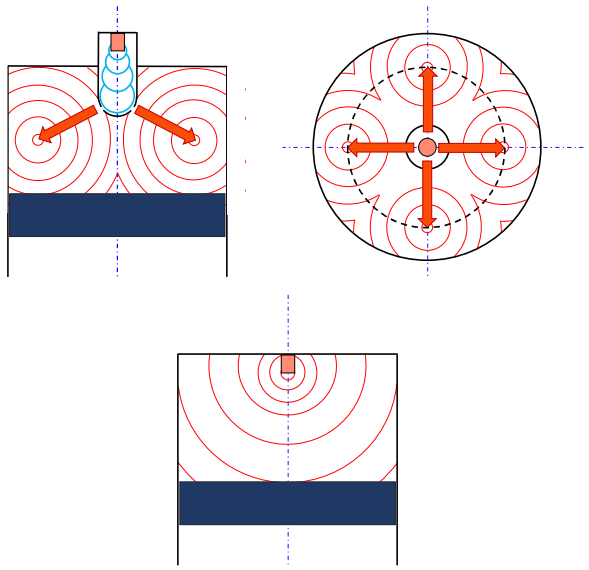

Figure 5. Flame front schematizations for PC engine (top) and conventional engine (bottom).

Three different correlations are used for the estimation of the laminar flame speed, S_L in Eq. (3), depending of the fuel injected. For the MC, a simulation-derived correlation for a TRF gasoline blend is utilized for all the tested architecture [34]. The same formulation is also applied for a passive PC. For the active pre-chamber, the correlations proposed in [35] and [36] are employed for the combustion of CNG and H_2, respectively. In the active PC, the possibility of fuel blending due to the mass exchange through the holes, is not taken into account in the model. In the next developments of the approach, laminar flame speed correlations for fuel blends or techniques for estimating the speed from the ones of pure fuels will be examined [35,37].

For the model closure, an "in-house developed" turbulence sub-model [38] is used, from which the values of L_{max}, L_{min}, and u' in both the chambers are derived. This sub-model belongs to the *K-k-T* family and describes the energy cascade mechanism from the mean flow kinetic energy, K, to the turbulent one, k, also taking into account a balance equation for the tumble angular momentum, T. Additionally, it describes the turbulence production in the chambers, induced by the incoming/outcoming flow through the orifices [39]. The accuracy and the tuning procedure of the turbulence model for the considered PC engine was presented in a previous authors' work [39]. This was carried out through the assessment with 3D simulation results. The same set of constants is here used for the conventional engine, not being available dedicated 3D simulations.

A Hohenberg-like correlation is employed for the heat transfer in the pre- and main-chamber [40], neglecting the heat losses in the PC holes. The gas-cylinder wall heat transfer in the PC is assumed to be controlled only by the pre-chamber pressure and temperature. Whereas, for the MC an additional dependence on the mean piston speed is considered.

The combustion model includes 3 tuning constants for each chamber. They act respectively on the flame wrinkling, c_{wrk}, on the transition between an initially-laminar and a fully-turbulent combustion, c_{trans}, and on the combustion tail, x_{wc}, [32]. For a divided-chamber engine, the above constants can be set independently for both PC and MC. Moreover, two additional tuning parameters are introduced for controlling the combustion transition between the two chambers. The former, r_{crit}, as mentioned before, triggers the MC combustion start, while the latter, c_{jet}, acts on the burn enhancement due to jets penetration in the MC. Hence, the combustion model presents 8 constants for a divided-chamber engine, while it gives 3 constants for a conventional architecture. A sequential methodology is followed for the model tuning, concerning in a first stage the conventional engine, and then the PC engine. The next steps were done:

1. Firstly, the model is tuned with reference to the standard engine (no pre-chamber), following the procedure described in [32]. In this way, the values of 3 tuning constants (c_{wrk}, c_{trans}, and x_{wc}) are identified.
2. Secondly, the pre-chamber engine is tuned. In this stage, the constants c_{wrk} and x_{wc} are borrowed from step 1 and applied for the tuning of the MC combustion. c_{trans} for the MC is imposed equal to 0, under the hypothesis that the combustion begins in fully turbulent stage. The constants (c_{wrk}, c_{trans}, and x_{wc}) for the PC simulation are identified according to the procedure in [32]. Finally, the values of r_{crit} and c_{jet} are selected with the aim of reproducing the combustion onset and burning speed in the main-chamber at the beginning of the process.

Using a trial-and-error procedure, a single set of tuning constants has been identified, determining the lowest average experiment/simulation error for all the investigated configurations, especially with regard to the pressure cycles in both PC and MC.

Engine model validation

The model validation is done through an experimental/numerical comparison of all the operating points listed in Table 2. In particular, two engine layouts are tested, the former refers to a conventional SI engine, whereas the letter includes the pre-chamber in both active and passive versions.

A unique 0D/1D scheme is used for all the investigated engine architectures (standard and PC engine, both active and passive). The average pressure/temperature measured signals are imposed as boundary conditions at the intake and exhaust ambient to get the maximum experimental/numerical congruence. In this track, the experimental spark timing, injection timing and duration are imposed as simulation input data.

In a first stage, the model validation is discussed in terms of global performance through an experimental/numerical comparison, including the Root Mean Squared Error (RMSE) as a global indicator of the model accuracy. The air flow rate, depicted in Figure 6, is satisfactorily predicted, with all the investigated points within the error band ± 5%. The related RMSE of 3.1 kg/h denotes an accurate schematization of the intake and exhaust pipe geometry and a proper specification of the valve flow coefficients. The IMEP values, illustrated in Figure 7, are satisfactorily predicted, remaining in most cases in the allowable error band of ± 5%. The exhaust temperature, as shown in Figure 8, is affected by a certain systematic overestimation, with a RMSE of around 56.4 K. This is probably due to an underestimation of the heat exchange in the cylinders or in the exhaust pipes.

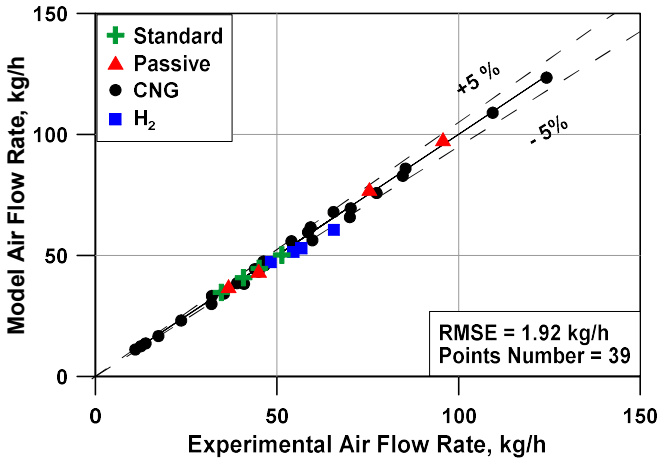

Figure 6. Experimental vs. numerical air flow rate comparison.

Concerning the combustion process description, since the spark timing is imposed in the simulations, the MFB_{50} can be considered as a measure of the combustion model overall reliability. Figure 9 underlines a satisfactory model accuracy, with an error within the band ± 5 CAD in most cases and an average of 2.4 CAD. A correct prediction of the combustion phasing and speed in both PC and MC is confirmed by the comparisons of the peak pressure angular location and level, depicted in Figure 10-Figure 11, respectively. The peak location is estimated better in the PC (RMSE equal to 2.09 CAD) than in MC case (RMSE equal to 2.83 CAD). In this last case, the prediction of the peak pressure level and timing appear more complex, since it depends on the superimposition of various effects (combustion

processes in both PC and MC). Results for the PC are more directly related to the spark timing, which is an imposed datum. Moreover, the air/fuel mixture quality in the PC is almost stoichiometric for all the considered operating conditions, while it widely changes in the MC among the different tested cases.

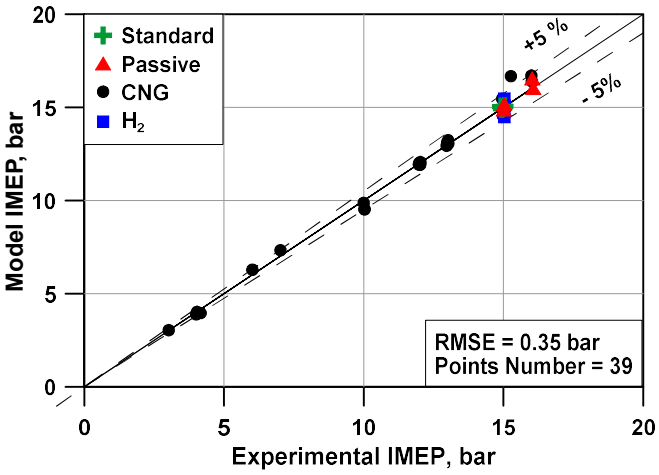

Figure 7. Experimental vs numerical IMEP comparison.

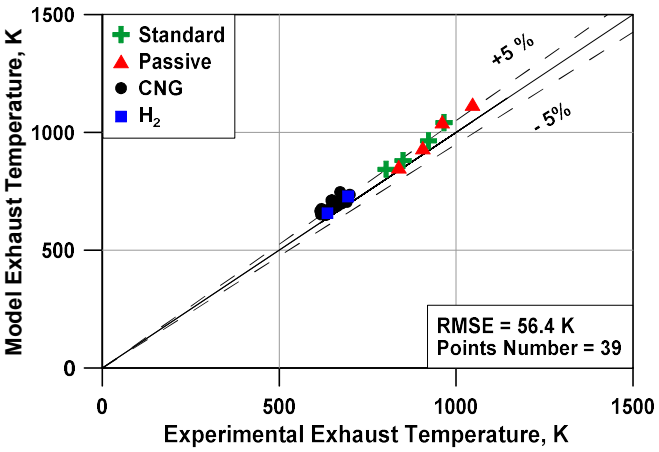

Figure 8. Experimental vs numerical exhaust temperature.

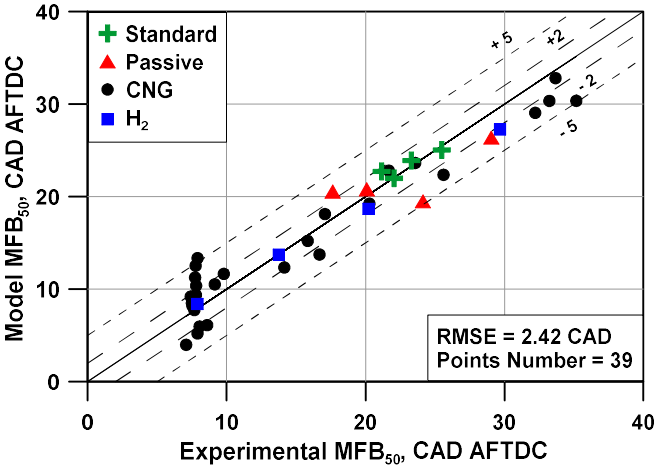

Figure 9. Experimental vs numerical MFB_{50} comparison.

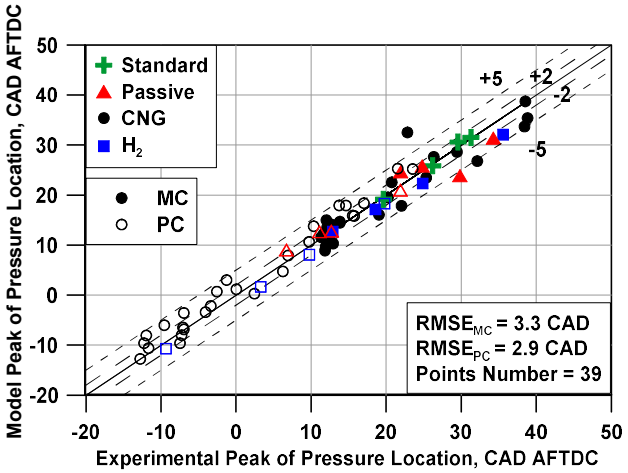

Figure 10. Experimental vs numerical peak of pressure angle for both MC and PC.

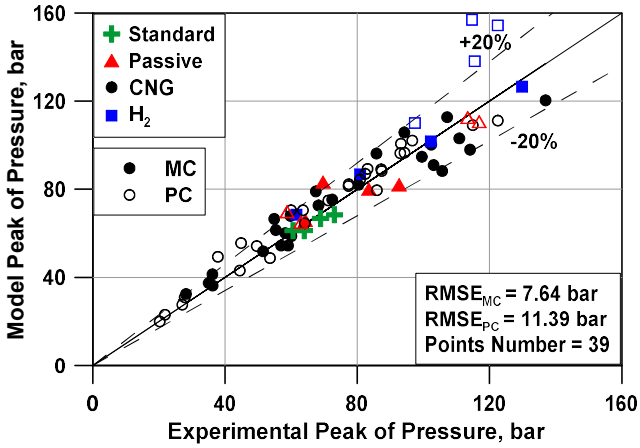

Figure 11. Experimental vs numerical peak of pressure for both MC and PC.

As an additional global verification of the combustion model reliability, in Figure 12 the combustion events against the mixture quality are reported for the various investigated engine architectures, for a representative low speed / high load operating point (2000 rpm @ 15 bar IMEP). The model produces very accurate predictions of all the combustion events for the standard architecture. For the pre-chamber device (both active and passive modes), the accuracy is rather satisfactory, with a certain underestimation of the combustion durations for the cases at reduced lambda. The combustion slow-down at leaning mixtures (more evident for the conventional architecture) is captured by the model mainly thanks to the decrement of the laminar flame speed. This behavior is compensated for the pre-chamber configurations, especially for the active version, by the effect of the turbulent jets arising from the PC. This is quite well captured by the model, as shown in Figure 12. As a final check of the simulation reliability, the experimental / numerical comparisons of the Indicated Thermal Efficiency (ITE) value are shown in Figure 13 for all the tested engine configurations once again in the operating point 2000 rpm @ 15 bar IMEP. All the data are normalized by the efficiency of the conventional engine under stoichiometric operation. The figure puts into evidence that the model well captures the efficiency improvement when λ increases, whatever is the considered ignition device.

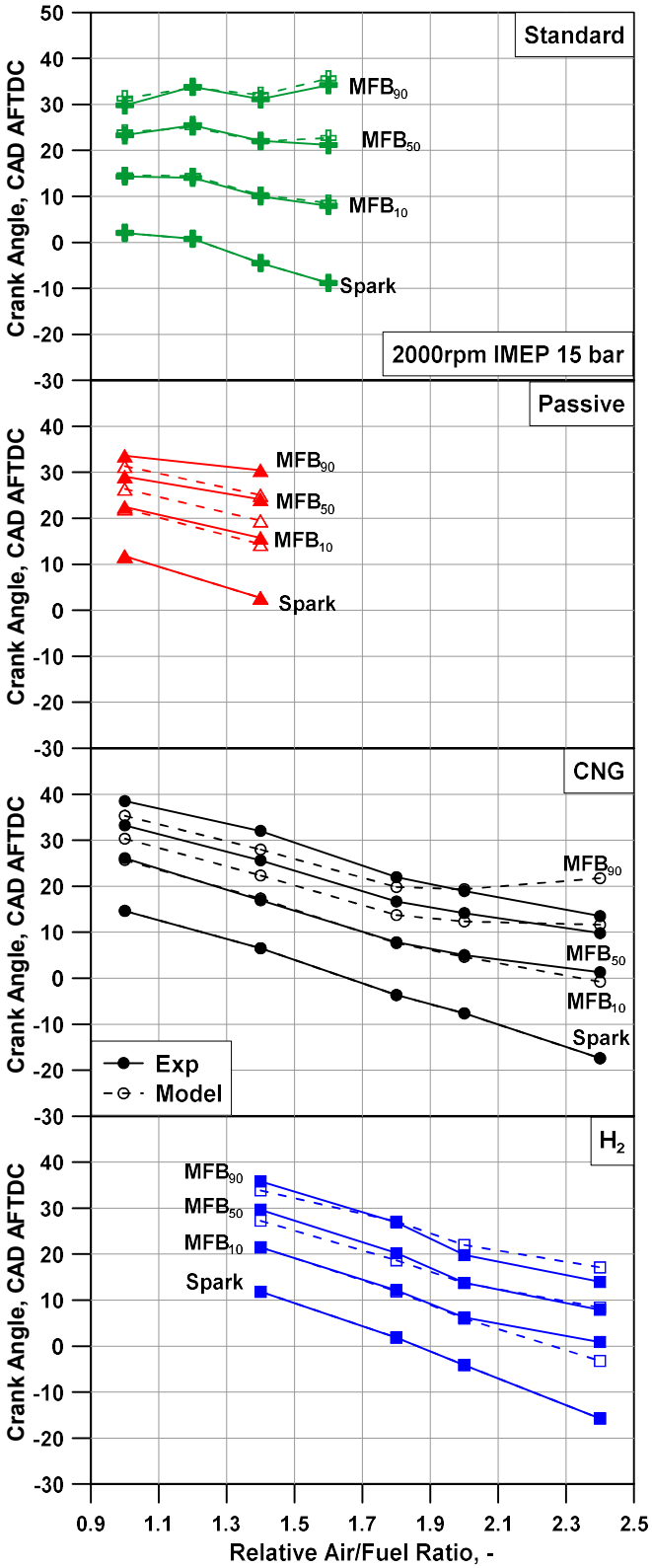

Figure 12. Experimental vs numerical combustion events for different air/fuel ratios at 2000 rpm @ 15 bar IMEP

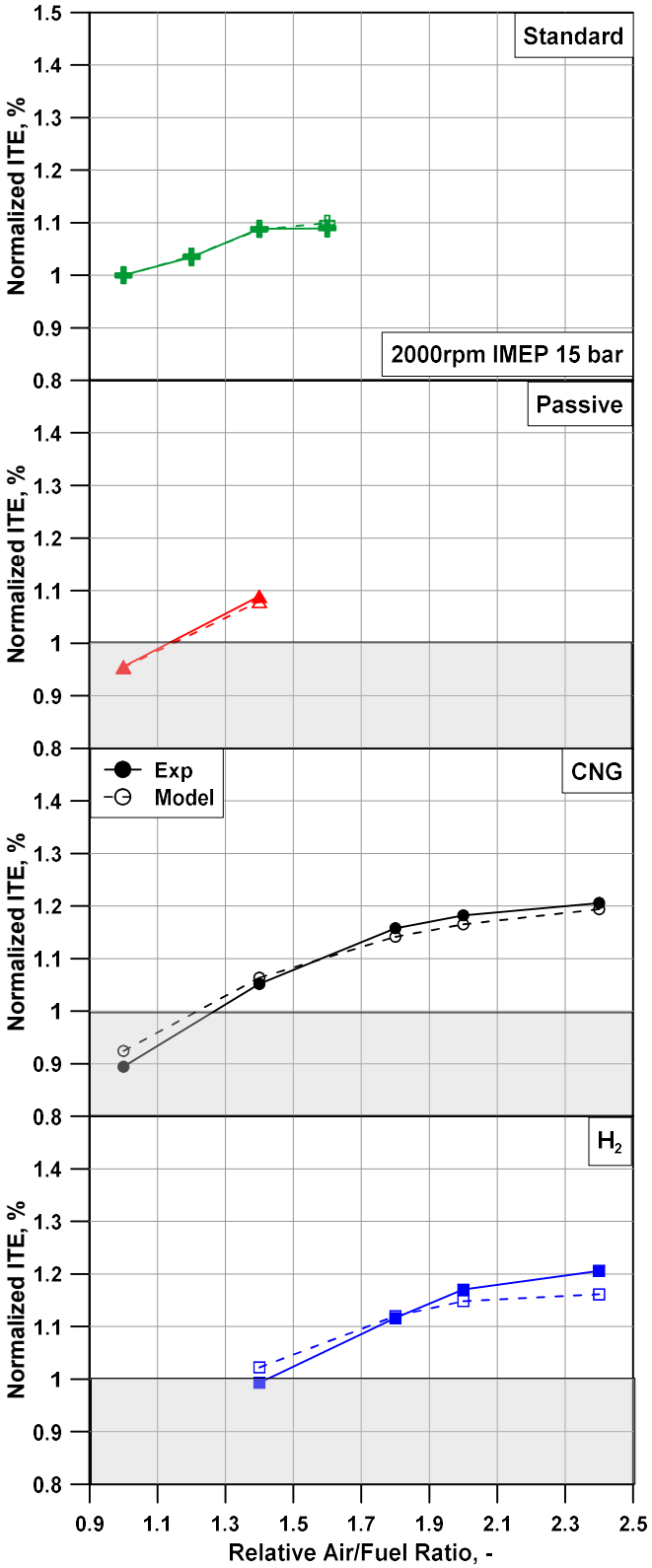

Figure 13 Experimental vs numerical normalized ITE for different air/fuel ratios at 2000rpm @ 15 bar IMEP.

Referring to the experimental data shown in Figure 12 and Figure 13, they clearly underline that the only way to work under very lean operations (λ greater than 1.6) is an active pre-chamber. This device demonstrates to consistently extend the lean burning limits. Another interesting outcome of the presented plots is that a standard ignition device is preferable in terms of efficiency if the engine works with a stoichiometric or slightly lean air/fuel mixtures. A pre-chamber becomes advantageous only for very lean operations, with λ above 1.8. The model, as stated above, demonstrates to capture this behavior with adequate accuracy.

As a final remark, the proposed results in terms of global performance parameter and combustion events demonstrate the consistency and reliability of the proposed numerical approach, considering the relevant variation range of operating conditions (speed, load and mixture quality) and the absence of a case-dependent model tuning.

A deeper insight in the combustion model reliability is given by the experimental / numerical comparisons of the pressure traces and of the related filtered burn rates, shown in Figure 14-Figure 18, for 15 representative cases. In those figures the experimental (numerical) data are represented with black (red) curves, continuous or dashed for the MC or PC, respectively.

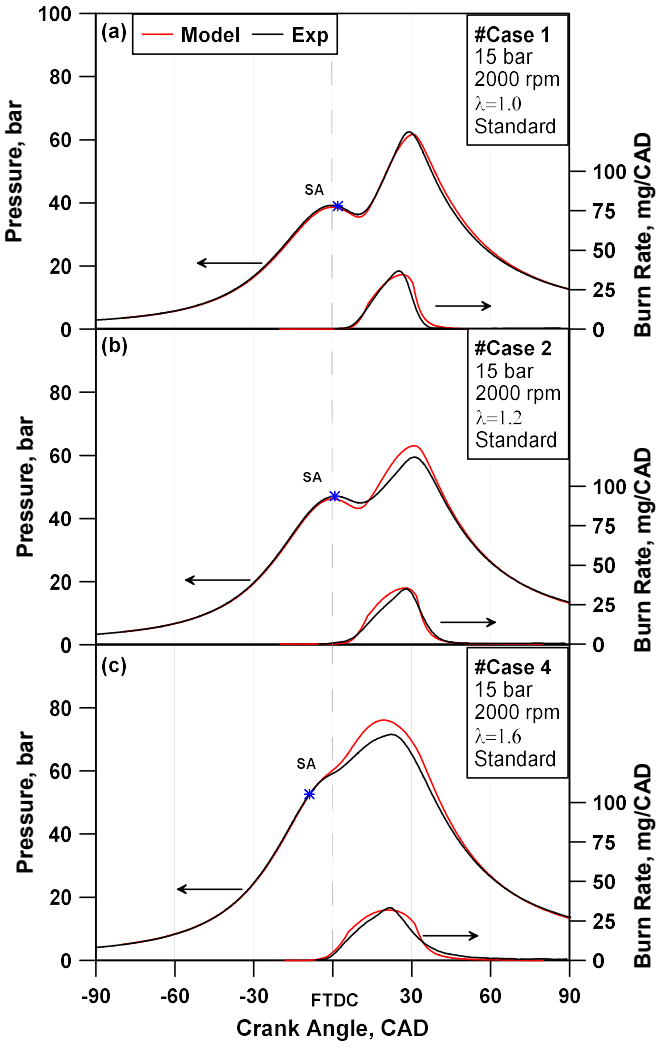

Figure 14. Experimental/numerical comparison of cylinder pressure traces and burn rates at 2000 rpm, 15 bar IMEP for a standard engine configuration, (a) λ=1.0, (b) λ=1.2, (c) λ=1.6.

In particular, in Figure 14 the conventional engine is investigated for a λ sweep at 2000rpm@15 bar. The experimental / numerical agreement is quite satisfactory for both pressure traces and burning rates. The model accuracy slightly worsens at increasing lambda, probably because of a reduced sensitivity of the adopted laminar flame speed correlation to the air/fuel mixture quality.

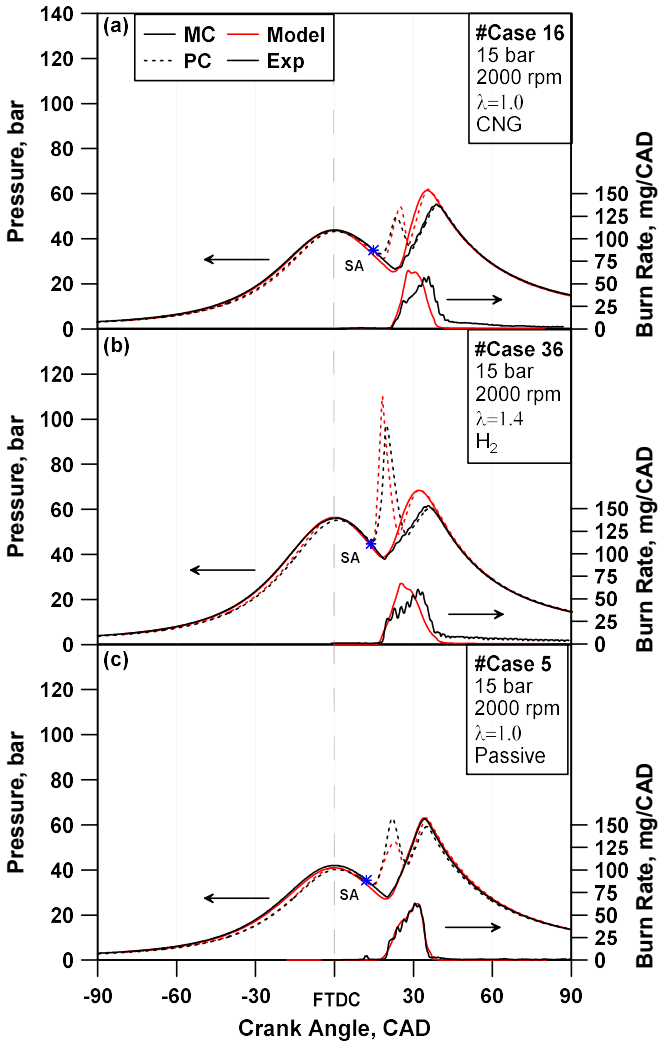

Figure 15. Experimental/numerical comparison of cylinder pressure traces and burn rates at 2000 rpm, 15 bar IMEP, (a) λ=1.0 CNG, (b) λ=1.4 H_2, (c) λ=1 passive.

In Figure 15, three injection configurations in the PC (CNG, H_2 and no injection) are compared at 2000rpm@15 bar for the less lean tested mixture quality. Analogous assessments are illustrated in Figure 16 for the same engine operating point and the leanest tested fuel metering. The model shows the capability to sense the main effects of the fuel type injected in the PC, detecting the maximum (minimum) burning speeds in the PC for H_2 (passive) mode. An intermediate behavior emerges for CNG PC fueling. The pressure peaks in both main- and pre-chamber are rather well predicted in most cases. The model generally overestimates the PC burning speed under H_2 operation probably not considering the possibility of fuel blending coming from the main-chamber.

The numerical burning rate in the MC in some cases (#20 and #39) reaches lower peaks than the experimental counterpart, compensated by a faster burning rate at the combustion beginning. The model well reproduces the pressure gap between PC and MC pressure traces

during the compression phases, thanks to a proper selection of the PC hole diameter and of its discharge coefficient. The comparison between Figure 15 and Figure 16 underlines the boosting increase needed to meet the load with lean mixtures, both in the numerical and experimental traces, for each engine architecture.

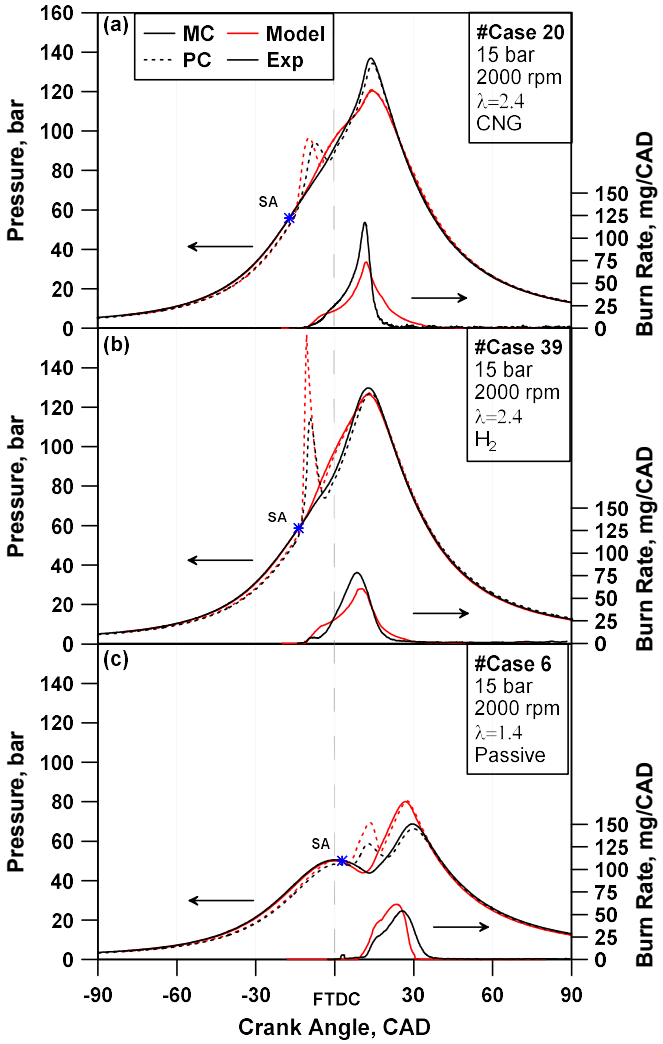

Figure 16 Experimental/numerical comparison of cylinder pressure traces and burn rates at 2000 rpm, 15 bar IMEP, (a) λ=2.4 CNG, (b) λ=2.4 H_2, (c) λ=1.4 passive.

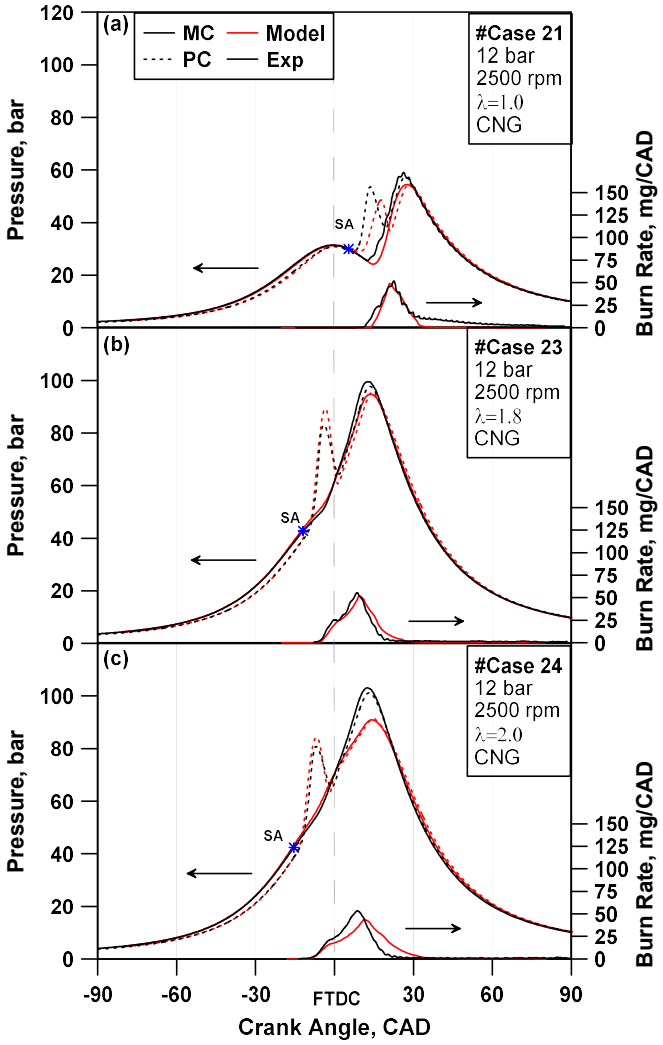

Figure 17. Experimental/numerical comparison of cylinder pressure traces and burn rates at 2500 rpm, 12 bar IMEP CNG fueled, (a) λ=1.0, (b) λ=1.4, (c) λ=2.0.

A more direct insight in the model sensitivity to mixture quality variations is given by the comparisons of Figure 17. This last concerns a representative medium/high load operating point (2500 rpm and 12 bar IMEP, CNG injected). The model capability in reproducing operations at medium loads and very lean λ is shown in Figure 18. In the assessments of Figure 17 and Figure 18, the pressure trends are quite well predicted in terms of global shape, phasing and location of the peaks in both MC and PC. In some cases, at lower loads (# 26 and 32), the PC pressure peak is overestimated, probably due to an incorrect simulation pre-chamber scavenging under these operations.

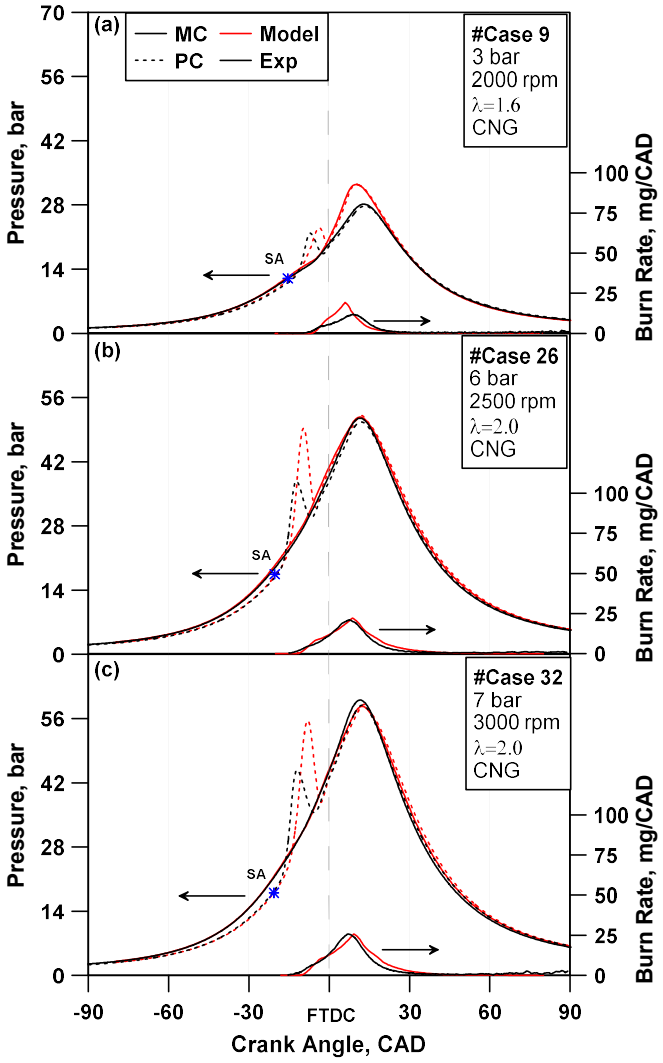

Figure 18 Experimental/numerical comparison of cylinder pressure traces and burn rates, CNG fueled, (a) λ=1.6 2000 rpm @3bar, (b) λ=2.0 2500rpm@6bar, (c) λ=2.0 3000rpm@7bar IMEP.

Conclusions

In this work, the potentialities of an ultra-lean pre-chamber SI engine was presented through numerical and experimental analyses. The experimental campaign was conducted at the VKA of RWTH Aachen University. The single cylinder engine under study was tested in four different layouts, including either a standard ignition device or a pre-chamber. 39 representative operating points with different engine loads, speeds and air/fuel mixture qualities were analyzed.

A 1D model of the tested engine was developed at the University of Naples, including refined phenomenological sub-models describing complex in-cylinder phenomena such as combustion, heat transfer, and turbulence. The fractal combustion model, suitable for a conventional SI engine, was properly extended to handle the divided combustion chamber architecture. The model takes into account the turbulence and burn rate enhancements due to the burned gas jets arising from the PC. The model accuracy was verified against the experimental pressure traces in both PC and MC and against the global engine performance parameters. The results underlined the good model capability in predicting air flow rate, IMEP and exhaust temperature, with a certain underestimation of the heat transfer. Concerning the pressure traces, the related burn rate profiles and the main combustion events, the experimental / numerical agreement is satisfactory, considering that the results were obtained without modifying the tuning constants for all the tested engine layouts and operating conditions.

The indicated thermal efficiency of the active pre-chamber, compared to the conventional engine, is strongly improved as emerged from both numerical and experimental results. Active PC devices gather greater advances thanks to the extension of the lean burning capability, compared to the passive PC or a standard spark plug. Next steps of the numerical activity will regard the handling of the combustions of fuel blends in the PC. Moreover, the model assessment will be extended over a wider engine operating domain so to underling the conditions where a PC is more effective for the efficiency improvement.

Contact information

References

1. European Environment Agency, “Annual European Union greenhouse gas inventory 1990–2016 and inventory report 2018,” Report No.:5/2018, 2018.
2. CO_2 emission standards for passenger cars and light-commercial vehicles in the European Union https://www.theicct.org/sites/default/files/publications/EU-LCVCO2- 2030_ICCTupdate_201901.pdf, The International Council on Clean Transportation. Last access date: 1 April 2019.
3. Saber, A., Venayagamoorthy, G., “Plug-in vehicles and renewable energy sources for cost and emission reductions,” *IEEE Transactions on Industrial electronics* 58.4 1229-1238,2011, doi:10.1109/TIE.2010.2047828.
4. Khaligh, A., Li, Z., “Battery, ultracapacitor, fuel cell, and hybrid energy storage systems for electric, hybrid electric, fuel cell, and plug-in hybrid electric vehicles: State of the art,” *IEEE transactions on Vehicular Technology*, *59*(6), 2806-2814, 2010, doi:10.1109/TVT.2010.2047877.
5. De Bellis, V., Bozza, F., Siano, D., Gimelli, A., “Fuel consumption optimization and noise reduction in a spark-ignition turbocharged VVA engine,” *SAE International Journal of Engines* 6(2): 1262-1274, 2013, doi:10.4271/2013-01-1625.
6. Roberts, M., “Benefits and Challenges of Variable Compression Ratio (VCR),” SAE Technical Paper 2003-01-0398, 2003, doi:10.4271/2003-01-0398.
7. Francqueville, L., Michel, J., “On the Effects of EGR on Spark-Ignited Gasoline Combustion at High Load,” *SAE Int J Engines* 7(4):1808-1823, 2014, doi:10.4271/2014-01-2628.
8. Hoppe, F., Thewes, M., Baumgarten, H., Dohmen, J., “Water injection for gasoline engines: Potentials, challenges, and solutions,” *International J of Engine Research* 17(1):86-96, 2016, doi:10.1177/1468087415599867.
9. Bozza, F., De Bellis, V., Teodosio, L., Tufano, D., Malfi, E., “Techniques for CO_2 Emission Reduction over a WLTC. A Numerical Comparison of Increased Compression Ratio, Cooled EGR and Water Injection,” SAE Technical Paper 2018-37-0008, 2018, doi:10.4271/2018-37-0008.

10. Germane, G., Wood, C., Hess, C., “Lean Combustion in Spark-Ignited Internal Combustion Engines - A Review," SAE Technical Paper 831694, 1983, doi:10.4271/831694.
11. Rapp, V., Killingsworth, N., Therkelsen, P., et al., “Lean Combustion, 2nd Edition,” (London, Lean-Burn Internal Combustion Engines, 2016), 111-146, doi:10.1016/C2013-0-13446-0.
12. Heywood, J., B., *“Internal combustion engine fundamentals*,” Vol. 930 (New York, Mcgraw-Hill, 1988), ISBN: 007028637X.
13. Moriyoshi, Y., Kuboyama, T., Kaneko, M., Yamada, T., Sato, H., “Fuel Stratification Using Twin-Tumble Intake Flows to Extend Lean Limit in Super-Lean Gasoline Combustion,” SAE Technical Paper 2018-01-1664, 2018, doi:10.4271/2018-01-1664.
14. Mazda Next-generation Technology, Skyactiv-X nextgeneration gasoline engine (press information, October 2017, https://insidemazda.mazdausa.com/press-release/mazda-nextgeneration-technology-press-information/.
15. Attard, W., Fraser, N., Parsons, P., Toulson, E., “A turbulent jet ignition pre-chamber combustion system for large fuel economy improvements in a modern vehicle powertrain,” *SAE International Journal of Engines*, 3(2), 20-37, 2010, www.jstor.org/stable/26275544.
16. Mueller, C., Morcinkowski, B., Habermann, K., Uhlmann, T., Schernus, C. “Development of a pre-chamber for spark ignition engines in vehicle applications,” 4th International Conference on Ignition Systems for Gasoline Engines, Dec. 2018.
17. Jamrozik, A., “Lean combustion by a pre-chamber charge stratification in a stationary spark ignited engine,” *Journal of Mechanical Science and Technology*, 29(5):2269-2278, 2015, doi:10.1007/s12206-015-0145-7.
18. Toulson, E., Schock, H., Attard, W., “A Review of Pre-Chamber Initiated Jet Ignition Combustion Systems,” SAE Technical Paper 2010-01-2263, 2010, doi:10.4271/2010-01-2263.
19. Lumsden, G., Watson, H., “Optimum Control of an S.I. Engine with a λ=5 Capability,” SAE Technical Paper 950689, 1995, doi:10.4271/950689.
20. Schumacher, M., Wensing, M., “A Gasoline Fuelled Pre-Chamber Ignition System for Homogeneous Lean Combustion Processes,” SAE Technical Paper 2016-01-2176, 2016, doi:10.4271/2016-01-2176.
21. Jamrozik, A., Tutak, W., Kociszewski, A., Sosnowski, M., “Numerical simulation of two-stage combustion in SI engine with prechamber,” *Applied Mathematical Modelling*, 37(5), 2961-2982, 2013, doi:10.1016/j.apm.2012.07.040.
22. Shah, A., Tunestål, P., Johansson, B., “CFD Simulations of Pre-Chamber Jets' Mixing Characteristics in a Heavy Duty Natural Gas Engine,” SAE Technical Paper 2015-01-1890, 2015, doi:10.4271/2015-01-1890.
23. Gentz, G., Thelen, B., Litke, P., Hoke, J., Toulson, E., “Combustion visualization, performance, and CFD modeling of a pre-chamber turbulent jet ignition system in a rapid compression machine,” *SAE International Journal of Engines*, 8(2), 538-546, 2015, doi:10.4271/2015-01-0779.
24. Biswas, S., Qiao, L., “A Numerical Investigation of Ignition of Ultra-Lean Premixed H_2/Air Mixtures by Pre-Chamber Supersonic Hot Jet,” *SAE Int. J. Engines* 10(5):2231-2247, 2017, doi:10.4271/2017-01-9284.
25. Hiraoka, K., Nomura, K., Yuuki, A., Oda, Y. et al., “Phenomenological 0-Dimensional Combustion Model for Spark-Ignition Natural Gas Engine Equipped with Pre-Chamber,” SAE Technical Paper 2016-01-0556, 2016, doi:10.4271/2016-01-0556.
26. Shojaeefard, M. H., Keshavarz, M. “Flame propagation model for a rotary Atkinson cycle SI engine,” *International Journal of Automotive Technology,* 19(1), 9-25, 2018, doi:10.1007/s12239-018-0002-7.
27. Auer, M., Wachtmeister, G. “Phenomenological models for pre-calculation of the combustion in gas engines,” MTZ worldwide, 70(6), 52-59, 2019, doi:10.1007/BF03226962.
28. Spindt, R., “Air-Fuel Ratios from Exhaust Gas Analysis,” SAE Technical Paper 650507, 1965, doi: 10.4271/650507.
29. Draper, S., “Pressure waves accompanying detonation in the internal combustion engine,” *Journal of the Aeronautical Sciences,* 5.6: 219-226, 1938, doi:10.2514/8.590.
30. De Bellis, V., Severi, E., Fontanesi, S., Bozza, F., “Hierarchical 1D/3D approach for the development of a turbulent combustion model applied to a VVA turbocharged engine. Part II: combustion model,” *Energy Procedia*, 45: 1027-1036, 2014, doi:10.1016/j.egypro.2014.01.108.
31. North, G., L., Santavicca, D., A., “The fractal nature of premixed turbulent flames,” *Combustion Science and Technology* 72(4-6): 215-232, 1990, doi:10.1080/00102209008951648.
32. De Bellis, V., Bozza, F., Tufano, D., “A Comparison Between Two Phenomenological Combustion Models Applied to Different SI Engines,” SAE Technical Paper 2017-01-2184, 2017, doi:10.4271/2017-01-2184.
33. Mastorakos, E., Allison, P., Giusti, A., De Oliveira, P., Benekos, S., Wright, Y., Boulouchos, K., “Fundamental Aspects of Jet Ignition for Natural Gas Engines,” *SAE International Journal of Engines*, doi:10.4271/2017-24-0097.
34. Bounaceur, R., Herbinet, O., Fournet, R., Glaude, P. et al., “Modeling the Laminar Flame Speed of Natural Gas and Gasoline Surrogates,” SAE Technical Paper 2010-01-0546, 2010, doi:10.4271/2010-01-0546.
35. Amirante, R., Distaso, E., Tamburrano, P., Reitz, R. D., “Laminar flame speed correlations for methane, ethane, propane and their mixtures, and natural gas and gasoline for spark-ignition engine simulations,” *International Journal of Engine Research*, 18(9), 951-970, 2017, doi:10.1177/1468087417720018.
36. Verhelst, S., Sierens, R., “A quasi-dimensional model for the power cycle of a hydrogen-fuelled ICE,” *International Journal of Hydrogen Energy*, 32(15), 3545-3554, 2007, doi: 10.1016/j.ijhydene.2007.02.011.
37. Dirrenberger, P., Gall, L., Bounaceur, R., Herbinet, O., Glaude, P., Konnov, A., et al. “Measurements of Laminar Flame Velocity for Components of Natural Gas,” *Energy & Fuels*, 25:3875–84, 2011, doi:10.1021/ef200707h.
38. Bozza, F., Teodosio, L., De Bellis, V., Fontanesi, S. et al., “A Refined 0D Turbulence Model to Predict Tumble and Turbulence in SI Engines,” *SAE Int. J. Engines* 12(1):15-30, 2019, doi:10.4271/03-12-01-0002.
39. Bozza, F., De Bellis, V., Tufano, D., Malfi, E., Müller, C., Habermann, K., “A Quasi-Dimensional Model of Pre-Chamber Spark-Ignition Engines,” SAE Technical Paper 2019-01-0470, 2019, doi:10.4271/2019-01-0470.
40. Hohenberg, G., “Advanced Approaches for Heat Transfer Calculations,” SAE Technical Paper 790825, 1979, doi: 10.4271/790825.

Acknowledgements

“This project has received funding from the European Union’s Horizon 2020 research and innovation programme under grant agreement No 724084”

Acronyms

0D-1D-3D	Zero-One-Three-dimensional
AFTDC	After firing top dead center
BTDC	Before top dead center

CAD	Crank angle degree
CFD	Computational fluid dynamics
CNG	Compressed natural gas
CO	Carbon monoxide
CO_2	Carbon dioxide
CoV	Coefficient of variation
DI	Direct injection
FFT	Fast fourier transformation
FTDC	Firing top dead center
H_2	Hydrogen
HC	Hydrocarbon
ICE	Internal combustion engine
IMEP	Indicated mean effective pressure
ITE	Indicated thermal efficiency
MC	Main-chamber
MFB	Mass fraction burned
NO_X	Nitrogen oxides
PC	Pre-chamber
RMSE	Root mean squared error
SA	Spark advance
SCE	Single cylinder engine
SI	Spark ignition
SPCCI	Spark-controlled compression ignition
TRF	Toluene reference fuel
VVA/VVT	Variable valve actuation / timing
WLTC	Worldwide harmonized Light vehicle Test Cycle
WLTP	Worldwide harmonized Light vehicle Test Procedure

Symbols

A_L, A_T	Laminar / turbulent flame area
B	Bore
c_{jet}	Fresh charge entrainment multiplier
c_{trans}	Laminar turbulent transition multiplier
c_{wc}	Wall combustion tuning multiplier
c_{wrk}	Wrinkling multiplier
D_3	Fractal dimension
f_0	Vibration frequency
k	Turbulent kinetic energy
K	Mean flow kinetic energy
L_{min}, L_{max}	Minimum / maximum flame front wrinkling scale
m	Mass
R	Gas constant
r_{crit}	PC critical radius for MC combustion start
S_L, S_T	Laminar / turbulent flame speed
T	Tumble angular momentum/Temperature
t	Time
u'	Turbulence intensity

Greeks

Λ_T	Taylor length scale
γ	Ratio of the specific heats
λ	Relative air/fuel ratio
ρ	Density/Vibration mode factor
τ	Entrainment characteristic time

Subscripts

10 / 50 / 90	Referring to 10 / 50 / 90% of mass fraction burned
b	Burned
cyl	Related to the cylinder
entr	Entrainment
fractal	Related to fractal approach
jet	Related to turbulent jet
m	Circumferential oscillation mode number
n	Radial oscillation mode number
u	Unburned

Superscripts

.	Temporal derivative